Satellite Products and Services Review Board

Algorithm Theoretical Basis Document: GCOM-W1/AMSR2 Sea Ice Product

Compiled by the
GCOM-W1/AMSR2 Sea Ice Team

Version 0.1

November 17, 2015

AUTHORS:

Walter N. Meier (NASA Goddard Space Flight Center)

J. Scott Stewart (National Snow and Ice Data Center)

Julienne Stroeve (National Snow and Ice Data Center)

DOCUMENT HISTORY
DOCUMENT REVISION LOG

DOCUMENT TITLE: ATBD – GCOM-W1/AMSR2 SNOW PRODUCT			
DOCUMENT CHANGE HISTORY			
Revision No.	**Date**	**Revision Originator Project Group**	**CCR Approval # and Date**
0.1	11/17/2015	W.N. Meier, J.S. Stewart, J. Stroeve	N/A

LIST OF CHANGES

DOCUMENT TITLE: ATBD – GCOM-W1/AMSR2 SNOW PRODUCT					
LIST OF CHANGE-AFFECTED PAGES/SECTIONS/APPENDICES					
Version Number	**Date**	**Changed By**	**Page**	**Section**	**Description of Change(s)**

TABLE OF CONTENTS

LIST OF TABLES

Page

LIST OF FIGURES

Page

LIST OF ACRONYMNS

AMSR2: Advanced Microwave Sounding Radiometer 2
AMSR-E: Advanced Microwave Scanning Radiometer for the Earth Observing System
AMSU: Advanced Microwave Sounding Unit
ARR: Algorithm Readiness Review
BT: Bootstrap sea ice concentration algorithm
CONUS: Continental United States
DDS: Data Distribution Server
EDR: Environmental Data Record
FAR: False Alarm Ratio
FOV: Field of View
GAASP: GCOM-W1 AMSR2 Algorithm Software Processor
GCOM – W1: Global Change Observation Mission 1st – Water
GR: Gradient ratio
IMS: Interactive Multisensor Snow and Ice Mapping System
JAXA: Japanese Aerospace Exploration Agency
MYI: Multi-year ice
MYIC: Multi-year ice concentration
NT2: NASA Team 2 sea ice concentration algorithm
NWS: National Weather Service
OSPO: Office of Satellite and Product Operations
PR: Polarization ratio
RMSE: Root Mean Square Error
SDR: Satellite Data Record
SIC: Sea ice concentration
SMMR: Scanning Multichannel Microwave Radiometer
SSMI: Special Sensor Microwave Imager
SSMIS: Special Sensor Microwave Imager and Sounder
TB: Brightness temperature

1. INTRODUCTION

1.1. Product Overview

1.1.1. Product Description

Sea ice is a key climate indicator due to its high albedo that reflects incoming solar radiation, its role as a physical barrier to heat and moisture transfer between the ocean and atmosphere, and its role in biogeochemical cycles. It is also plays a major role in polar ecosystems and in lives of indigenous peoples of the Arctic. Changes in Arctic sea ice over the past nearly four decades have been dramatic, with a loss of over a third of summer ice cover, a large decline in ice thickness, and a nearly-complete loss of old ice. Satellite remote sensing has been the primary tool for mapping sea ice concentration, extent, and age since the late 1970s. The Advanced Microwave Sounding Radiometer 2 (AMSR2) onboard the first Global Change Observation Mission – Water (GCOM-W1) satellite includes similar microwave frequencies that have been used for sea ice retrievals from previous sensors: Scanning Multichannel Microwave Radiometer (SMMR), and a series of Special Sensor Microwave Imagers (SSMI) and Special Sensor Microwave Imager/Sounders (SSMIS). These provide the continuous and consistent long-term record of sea ice beginning in late 1978. More recently, the Advanced Microwave Scanning Radiometer for the Earth Observing System (AMSR-E) provides improved spatial resolution and other advances and is a pre-cursor to AMSR2. The sea ice products based on AMSR2 microwave measurements include sea ice concentration (SIC), multi-year ice concentration (MYIC), and several quality indicator fields.

1.1.2. Product Requirements

AMSR2 sea ice products are generated using several AMSR2 microwave frequencies. Microwave radiation is unhindered by darkness and clouds and penetrates a deeper layer of snow cover unlike visible channels. However, microwave radiation has larger field of view than visible channels due to its limitation of antenna size and also microwave measurement has limitations on the snow depth retrieval due to its saturation with deep snow depth. AMSR2 observes the earth with the horizontal sampling interval of 10 km. Tables 1-1 and 1-2 show the product requirements for AMSR2 SIC and MYIC.

1.2. Satellite Instrument Description

AMSR2 is a microwave instrument that was launched in 2012 on board GCOM-W1 satellite. Now that GCOM-W1 is part of the “A-train” constellation along with Aqua and AMSR-E and AMSR2 have the same center frequencies and corresponding bandwidths, AMSR2 is considered as the successor to AMSR-E. AMSR-E is a passive microwave radiometer sensing microwave radiation at 6 frequencies ranging from 6.9 to 89.0 GHz with fields of view from approximately 5 to 50 km (Table 1-3). AMSR-E onboard the polar-

orbiting satellite (Aqua) operationally provided sea ice properties (concentration, snow depth on sea ice, and drift; Comiso et al., 2003; Markus and Cavalieri, 2009) until it failed in regular scanning due to an antenna problem in October 2011. However, AMSR2 has several enhancements: larger main reflector, additional 7.3 GHz channels, an improved calibration system (Imaoka et al., 2010), and improved spatial resolution (Table 1-3). Level 1R full-orbit of AMSR2 brightness temperature products (L1SGRTBR) are used in the original delivery.

Table 1-1: Requirements for the NOAA GCOM-W1/AMSR2 sea ice concentration.

EDR Attribute	Threshold	Objective
Applicable conditions	Delivered under "all weather" conditions	Delivered under "all weather" conditions
Horizontal cell size	10 km	5 km
Mapping uncertainty, 3 sigma	5 km	3 km
SIC and MYIC Range	0 – 100 %	0 – 100%
Measurement uncertainty	10 %	5 %
Refresh	At least 90% coverage of the globe about every 20 hours (monthly average)	Not Specified

2. ALGORITHM DESCRIPTION

The primary sea ice concentration algorithm is the NASA Team 2 (NT2) algorithm (Markus and Cavalieri, 2000). The algorithm is an enhancement to the original NASA Team algorithm (Cavalieri et al., 1984) that adds the high-frequency (89 GHz) channels to reduce sensitivity to surface inhomogeneity. The method is iterative where modeled brightness temperatures for different atmospheric conditions are adjusted to minimize a cost function of the difference between the model and observed brightness temperatures. The minimum cost function is the sea ice concentration solution. This approaches provides the best atmospheric correction (from 12 standard atmospheres) to account for the greater sensitivity of the 89 GHz to atmospheric emission. The Bootstrap (BT) algorithm is also computed as a secondary concentration estimate, albeit without post-processing QC.

Therefore, the BT parameter should not be used for concentration estimates. The main purpose of including the BT algorithm is as input to the NT2-BT concentration difference field, which provides an estimate of concentration uncertainty.

Table 1-1: Requirements for the NOAA GCOM-W1/AMSR2 multi-year ice concentration.

EDR Attribute	Threshold	Objective
Applicable conditions	Delivered under "all weather" conditions	Delivered under "all weather" conditions
Horizontal cell size	10 km	5 km
Mapping uncertainty, 3 sigma	5 km	3 km
Measurement range	0 – 100 %	0 – 100 %
Measurement uncertainty	70% probability of correct typing of ice age class	90 %
Refresh	At least 90% coverage of the globe about every 20 hours (monthly average)	Not Specified

Table 1-2: Comparison of AMSR2 and AMSR-E (Imaoka et al. 2010) features.

AMSR2	**Center Freq (GHz)**	**6.9/7.3**	**10.7**	**18.7**	**23.8**	**36.5**	**89.0**
	Band Width (MHz)	350	100	200	400	1000	3000
	IFOV (km x km)	35x62	24x42	14x22	15x26	7x12	3x5
AMSR-E	**Center Freq (GHz)**	**6.9**	**10.7**	**18.7**	**23.8**	**36.5**	**89.0**
	Band Width (MHz)	350	100	200	400	1000	3000
	IFOV (km x km)	43x75	29x51	16x27	18x32	8x14	4x6

2.1. Processing Outline

The processing for the sea ice product retrieval provides SIC, MYIC, and quality fields based on AMSR2 brightness temperature and several ancillary data (Figure 2-1). The

processing of the algorithm is run for each new swath of L1R input brightness temperatures; however, all of the output fields are gridded on polar subsets of a 10 km EASE2 Grid (Brodzik et al., 2012; 2014; https://nsidc.org/data/ease/ease_grid2.html). The NT2 concentration and MYIC are calculated for each swath and then gridded, while the BT concentration is calculated on gridded TB fields. The gridding is done using a drop-in-the-bucket approach using the most recent TB swath observation. When a newer TB comes in for a given grid cell, the newer concentration replaces the older value. The latest observation for each cell is tracked in a gridded latency field.

2.2. Algorithm Input

The AMSR2 sea ice concentration algorithm requires AMRS2 L1R brightness temperatures between 18.7 GHz to 89 GHz. Required ancillary inputs include: land mask, coast mask, and monthly ocean SST climatology mask; all masks are gridded on the EASE2 polar subset grid. The SST climatology masks were originally the NSIDC polar stereographic projection and have been re-projected to the EASE2 use NSIDC Mapx tools. The land and coast masks were re-derived from a land-ocean-coast-ice mask derived from Boston University MODIS/Terra land cover dataset (Brodzik and Knowles, 2011; Friedl et al., 2002; http://nsidc.org/data/docs/daac/nsidc0609/). The Antarctic land mask was further modified from updated shapefiles provided by Terry Haran (NSIDC) based on an updated mask produced by the U.S. National Ice Center in Suitland, MD. The updated land mask accounted for changes in Antarctic ice shelves.

- Land masks: While the AMSR2 TB fields do include a land flag for each sensor footprint, the gridded land mask is instead used here because the TB land flag is out of date and does not account for changes in ice shelves in Antarctica, such as the Larsen-B.

- Coast masks: Defines grid cells adjacent to and near the land-ocean boundary. This is used to do a land-spillover correction needed to remove false ice along the coast, which occurs because under some conditions a mixed water-land grid cell (i.e., a cell that contains sensor footprints from partly over open water and partly over land) will seen by the SIC algorithms as being ice-covered.

- Ocean SST masks: Weather filters (described below) do not remove all spurious (e.g., due to wind roughening on the surface) and ice can potentially occur in regions that clearly cannot have sea ice (e.g., off the coast of Spain). Thus an additional mask is applied based on a monthly SST climatology from Levitus and Boyer (1994). There are masks for each month and each hemisphere (24 total mask files), each using an SST threshold to mask out regions of “no possible ice”. The threshold in the Arctic is 278 K and in the Antarctic is 275 K.

2.3. Theoretical Description

2.3.1. Sea Ice Microwave Properties

The microwave electromagnetic properties of sea ice are a function of the physical properties of the ice, such as crystal structure, salinity, temperature, or snow cover. In addition, open water typically has an electromagnetic emission signature that is distinct from sea ice emission (Eppler et al., 1992). These properties form the basis for passive microwave retrieval of sea ice concentrations.

Specifically, the unfrozen water surface is highly reflective in much of the microwave regime, resulting in low emission. In addition, emission from liquid water is highly polarized. When salt water initially freezes into first-year (FY) ice (ice that has formed since the end of the previous melt season), the microwave emission changes substantially; the surface emission increases and is only weakly polarized. Over time as freezing continues, brine pockets within the sea ice drain, particularly if the sea ice survives a summer melt season when much of the brine is flushed by melt water. This multi-year (MY) ice has a more complex signature with characteristics generally between water and first-year ice. Other surface features can modify the microwave emission, particularly snow cover, which can scatter the ice surface emission and/or emit radiation from within the snow pack. Atmospheric emission also contributes to any signal received by a satellite sensor. These issues result in uncertainties in the retrieved concentrations, which are discussed further below.

Because of the complexities of the sea ice surface as well as surface and atmospheric emission and scattering, direct physical relationships between the microwave emission and the physical sea ice concentration are not feasible. Thus, the standard approach is to derive concentration through empirical relationships. These empirically derived algorithms take advantage of the fact that brightness temperature in microwave frequencies tend to cluster around consistent values for pure surface types (100% water or 100% sea ice). Concentration can then be derived using a simple linear mixing equation for any brightness temperature that falls between the two pure surface values:

$$TB = T_{SI} \times C_{SI} + T_{OW} \times (1 - C_{SI}) \quad (1)$$

Where T_B is the observed brightness temperature, T_I is the brightness temperature for 100% sea ice, T_{OW} is the brightness temperature for open water, and C_{SI} is the sea ice concentration. The equation can be inverted to solve for C_{SI}.

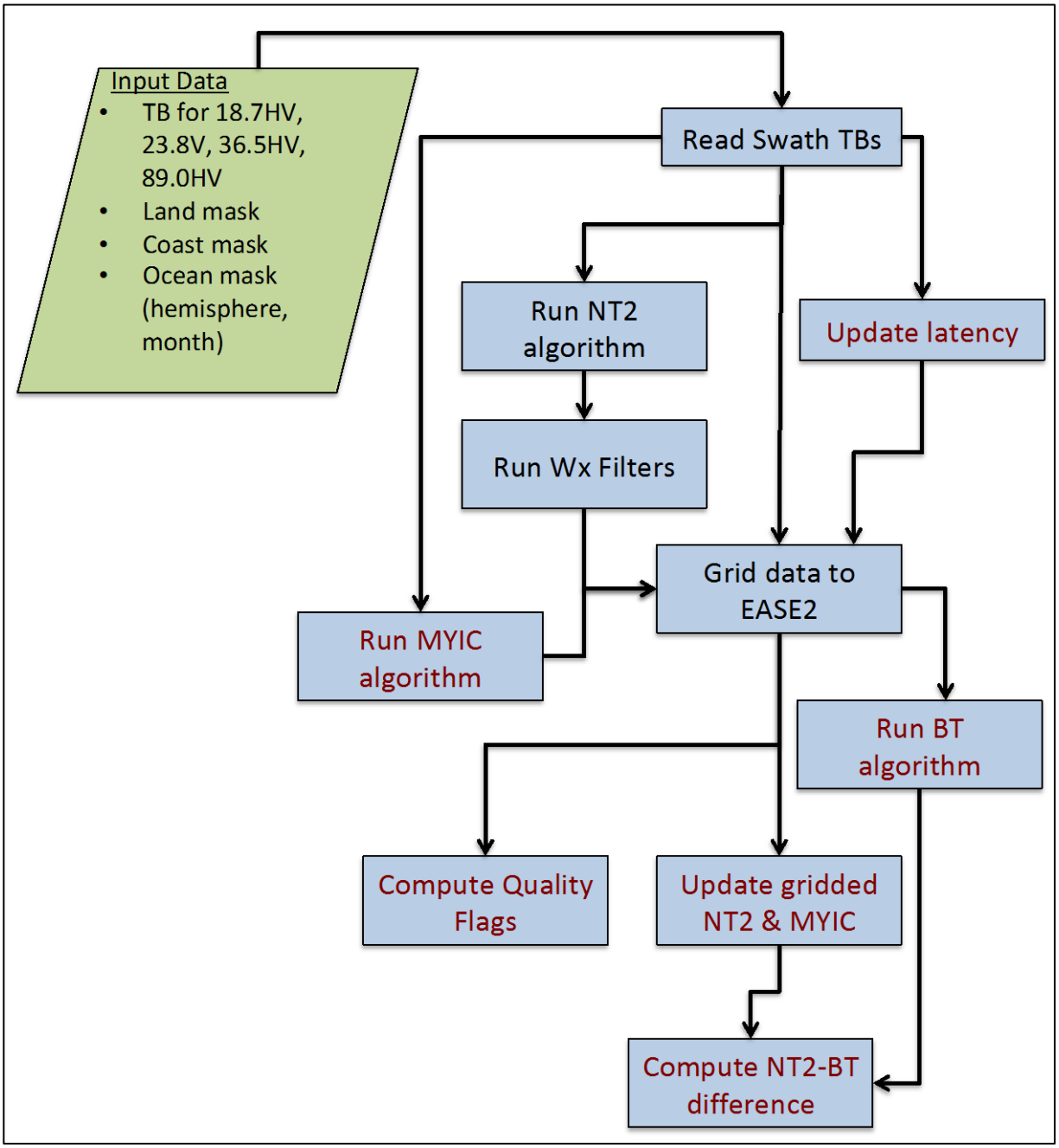

Figure 2-1: Processing outline for AMSR2 snow property retrieval algorithm. Steps leading to output fields are in red text.

In reality, such an approach is limited by the surface ambiguities and atmospheric emission. Using combinations of more than one frequency and polarization limits these effects, resulting in better discrimination between water and different ice types and a more

accurate concentration estimate. This has been the general approach for most sea ice algorithms – using differences and/or ratios between different TB frequencies and polarizations. However, the NT2 algorithm takes a different approach.

2.3.2. NASA Team 2 Sea Ice Concentration Algorithm

The NASA Team 2 algorithm (Markus and Cavalieri, 2000) was developed for AMSR-E (Comiso et al., 2003) as an enhancement to the original NASA Team algorithm (Cavalieri et al., 1984). At its most basic, NT2 is similar in structure to NT, using polarization ratios (PR) and gradient ratios (GR). These are ratios TB differences between two frequencies (GR) or two polarizations (PR), normalized by the sum of the TBs, as in:

$$PR(\nu) = \frac{[TB(\nu,V) - TB(\nu,H)]}{[TB(\nu,V) + TB(\nu,H)]} \quad (2)$$

$$GR(\nu_1, \nu_2, p) = \frac{[TB(\nu_1,p) - TB(\nu_2,p)]}{[TB(\nu_1,p) - TB(\nu_2,p)]} \quad (3)$$

where ν is frequency, p is polarization (H = horizontal, V = vertical). The actual radiance ratios used in the NT2 algorithm are $PR_R(18)$, $PR_R(89)$, GR (89, 18, H), and GR (89, 18, V) where the subscript R refers to a rotation of axes. This rotation is done in the PR(18)-GR(37, 18, V) domain, with the axes rotated through an angle, φ, until the ice-type lines (the FY-MY line for the Arctic and the A–B line for the Antarctic) are parallel to the GR axis. The rotated PR is defined by:

$$PR_R(18) = -GR(37V18V)\sin\phi + PR(18)\cos\phi \quad (4)$$

$$\Delta GR = GR(89,18,H) - GR(89,18,V) \quad (5)$$

The axis rotation (ϕ) is one new enhancement from NT, as the use of the 89 GHz frequency. An issue for using 89 GHz for sea ice is stronger atmospheric emission at this frequency. Thus a third parameter is defined to avoid the ambiguity between changes in sea ice concentration and changes in atmospheric conditions, because of the higher sensitivity of the 89-GHz channels to atmospheric variability compared to the lower frequency channels. This third parameter is the rotated PR(89), $PR_R(89)$, computed from the PR(89)-GR(37V18V) domain analogous to the calculation of $PR_R(18)$ but with a different angle.

The most significant difference between NT2 and NT is the use of a forward atmospheric radiative transfer model (Kummerow, 1993) to quantify atmospheric effects. This is done by calculating brightness temperatures for each channel by using the model and incorporating four surface types: first-year ice, multiyear ice, Type C (which corresponds to thin ice or ice with thick snow cover), and open water. Thus, the 89 GHz channels together with a forward radiative transfer model provide ice concentrations under different atmospheric conditions.

Figure 2-2 shows the general flow of the algorithm. First brightness temperatures are calculated for the four surface types and twelve different atmospheric conditions. The response of the brightness temperatures to different atmospheres is calculated using the atmospheric radiative transfer model.

The input data for the model consists of several things such as: the emissivities of the different surface types taken from Table 4-1 in Eppler et al. (1992) with modifications to achieve agreement between modeled and observed ratios, different cloud properties, specifically cloud base, cloud top, and cloud liquid water, taken from Fraser et al. (1975), and average atmospheric temperature and humidity profiles for summer and winter conditions taken from Antarctic research stations. Brightness temperatures are calculated for all possible ice concentration combinations in one percent increments, and the following ratios were calculate for each increment: $PR_R(18)$, $PR_R(89)$, and ΔGR. This creates a prism in which each element within this space contains a vector with the three ratios: $PR_R(18)$, $PR_R(89)$, and ΔGR. The subscript R refers to a rotation of axes in PR-GR space by the angle so that $PR_R(18)$ and $PR_R(89)$ are independent of ice types A and B in the Antarctic, and first-year and multiyear ice for the Arctic. For each pixel, the observed brightness temperatures are used to create a vector with the same ratios. The ice concentration for a pixel is determined where the difference between an observed and a modeled ratio is smallest.

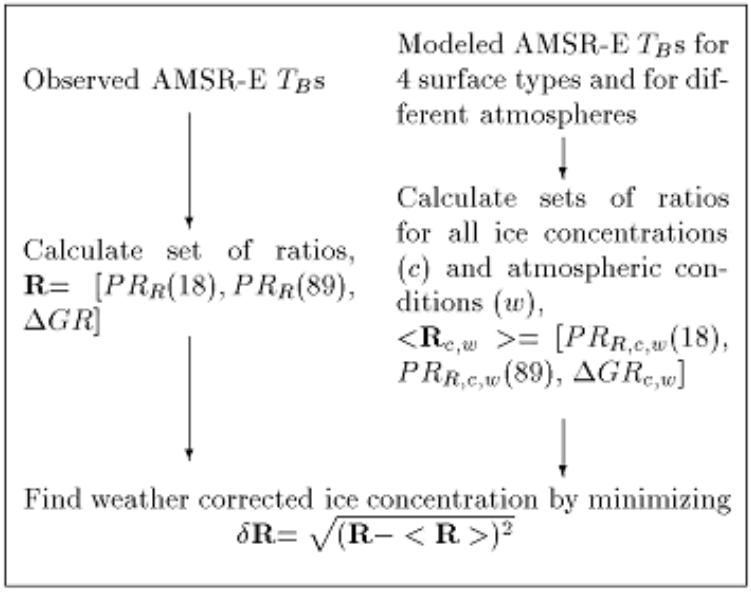

Figure 2-2. Flow diagram of NASA Team 2 algorithm.

Weather effects have been mentioned above. These are most notably strong atmospheric emission (primarily liquid water, water vapor) and/or surface scattering/emission (due to wind roughening of the ocean surface over the open ocean. This results in sea ice

retrievals over the open water because of the sensitivity to the channels and ratios to these effects. To ameliorate these effects, two weather filters were developed, using GR thresholds of 0.05 for GR(37V,18V) and 0.045 for GR(22V,18V); if either of the GR values are above the threshold for a grid cell, sea ice concentration is set to zero for that grid cell. In examining consistency between AMSR2 and AMSR-E (more detail below), it was found that adjusting the GR(37V,18V) to 0.046 provide the best consistency between the sensors and thus 0.046 is used for GR(37V,18V) in this AMSR2 sea ice product.

2.3.3 Multi-Year Sea Ice Concentration

The multi-year ice concentration (MYIC) algorithm implemented here is experimental and was derived at NASA Goddard (L. Brucker and D. Cavalieri) during further investigations using the NT2 algorithm. As such it is a research product and requires further validation. Thus for the purposes of this product, it should be considered “beta” and used with caution. In addition, the algorithm is only valid for the Arctic during winter, where the signatures of MYI and FYI are distinct. In Antarctica, there is little MYI and the character is different, so MYIC algorithms do not have high confidences in the Antarctic. However, initial investigation, suggests that the algorithm may be able to retrieve reasonable indications of MYI. During the melt season, melting snow and surface water on the ice, obscures the MYI and FYI signatures and the algorithm does not yield valid results. Validation of the MYIC product is currently underway. When results are available, they will be published in a peer-reviewed journal and this document will be updated.

Essentially, the MYIC algorithm uses the fact that the gradient ratio is sensitive to the presence of multi-year ice, as was seen in the original NT algorithm. The MYIC is a ratio of GR(37V,18V) values with coefficients (tiepoints) based on pure surface types.

$$C_{MY} = \frac{[E(GR-1)+F(GR+1)]}{[A(GR-1)+B(GR+1)]} \quad (6)$$

where GR is GR(37V,18V) and:

$$A = TB(37V)_{MY} - TB(37V)_{FY} \quad (6a)$$

$$B = TB(18V)_{MY} - TB(18V)_{FY} \quad (6b)$$

$$E = TB(37V)_{OW} \times (1 - C_{tot}) + TB(37V)_{FY} \times C_{tot} \quad (6c)$$

$$F = TB(18V)_{OW} \times (1 - C_{tot}) + TB(18V)_{FY} \times C_{tot} \quad (6e)$$

The TB values in Equation 6 are tiepoints empirically derived for pure surface types – MY, FY, and open water (OW) – and are given as:

$$TB(18V)_{MY} = 237.6\ K$$
$$TB(37V)_{MY} = 218.9\ K$$
$$TB(18V)_{FY} = 254.8\ K$$
$$TB(37V)_{FY} = 248.9\ K$$
$$TB(18V)_{OW} = 237.6\ K$$
$$TB(37V)_{OW} = 218.9\ K$$

2.3.4 Bootstrap Sea Ice Algorithm

The Bootstrap (BT) sea ice algorithm is included in the product as a secondary concentration field and is intended only as an input to ancillary output fields of data quality indications, primarily as part of the Concentration Difference (NT2-BT) field. The difference field provides an indication of uncertainty because differences are expected be larger where errors/uncertainties in concentration are higher. A key point on the BT concentration parameter is that it does not include the weather filters or SST masks used for QC of the NT2 estimates. Thus, the BT field will potentially have many regions of spurious ice cover.

Because the BT is not a primary algorithm, it is not described in detail here. Detailed information on the algorithm can be found in Comiso et al. (2003), Comiso and Nishio (2008), and Comiso (2009).

2.4. Algorithm Output

The output of the algorithm is given in Table 2-1. All fields are on the 10 km EASE2 polar subset grid with grid size of 1050 x 1050 for the Arctic (Northern Hemisphere grid) and 840 x 840 for the Antarctic (Southern Hemisphere grid).

2.5. Performance Estimates

2.5.1. Algorithm validation

The NT2 algorithm used here has been directly adapted from the NASA AMSR-E product suite code, which is archived at NSIDC (http://nsidc.org/data/ae_si12). Ten years of AMSR-E products were produced and significant validation was done on the algorithm for AMSR-E (Cavalieri et al., 2006). In addition, numerous evaluations and intercomparisons of the NT2, BT, and other algorithms have been done by various groups, including Meier (2005), Andersen et al. (2006; 2007), and Ivanova et al. (2014; 2015). Thus a though validation was not done for this version of the product although the algorithms were previously validated.

Table 2-3: Output structure of GCOM/AMSR2 Sea Ice EDR.

EDR Output	Description	Dynamic Range
NT2 SIC	Primary sea ice concentration estimate	0 – 100 %
BT SIC	Secondary sea ice concentration estimate (no QC)	0 – 100 %
NT2-BT SIC	Difference between NT2 and BT concentrations	-100 – +100 %
SIC Range	Range of NT2 concentration over 24 hours (max – min concentration)	0 – 100 %
Age of observation	Age of observation on which concentration is based	0 – 1440 minutes
MYIC	Multi-year sea ice concentration (provisional)	0 – 100 %
Quality Flag Field	Bitwise combination of quality conditions: 4: SST limited (SST mask applied) 8: Weather limited (weather filter threshold exceeded) 16: Land-spillover corrected (coastal ice removed) 32: Spatially interpolated (missing grid cells bi-linearly interpolated) 64: Missing (no valid TBs found) 128: Land	[4, 8, 16, 32, 64, 128]

There are two primary differences between this product and the NASA AMSR-E product. The first is that this product uses only the most recent observation at a given grid cell instead of all observations over a 24-hour period. Overall, this change is expected to be minimal except in a few cells near the ice edge where ice is actively growing, melting or potentially advecting in and out cells. An assessment comparing to the two methods confirmed this with differences of at most a few percent within the ice pack and only a grid cell or two wide fringe at the ice edge where differences are larger. The Concentration Range field included in this product provides an indication of this time effect.

The second and more important difference is that this product is for AMSR2, not AMSR-E and sensor differences result inconsistencies and possibly other errors in the output. This was addressed by using a thorough intercalibration done at NASA Goddard to adjusted the AMSR2 TBs to be consistent with the AMSR-E based code. This was done via a regression of AMSR2 TBs with AMSR-E 2 rpm data. Regressions were done at all AMSR-E 2 rpm footprints in and near sea ice covered ocean regions. Regressions were done independently for the Arctic and Antarctic regions each day for a full year. The daily regressions were averaged into monthly regression coefficients. The monthly regressions were found to be reasonably consistent over the year, so they were averaged to a single regression equation for each TB frequency and polarization. These coefficients are applied to the AMSR2 TBs after they are read in and before they are input into the concentration algorithms.

The consistency between the concentration fields using the regressed AMSR2 TBs and AMSR-E cannot be directly tested over complete sea ice fields because AMSR-E ceased regular operations before the launch of AMSR2 and only sparse data from the 2 rpm operation are available. Thus to investigate consistency, the AMSR2 and AMSR-E fields were compared with SSMIS SIC. Because the SSMIS is from the same sensor the concentration estimates are consistent and thus it provides a useful baseline for comparing AMSR2 and AMSR-E. If the AMSR2-SSMIS difference is consistent with the AMSRE-SSMIS difference, then via a double-differencing approach, the AMSR2-AMSRE match can be determined.

This was done for a full year (2010 for AMSRE, 2013 for AMSR2) using the total sea ice extent as a measure of consistency. While the TB regression substantially improved the AMSR2 consistency with AMSR-E, there was still some remaining bias. This was found to be due primarily to weather effects, indicating that the GR(37V,18V) weather filter threshold needed adjusting. As noted above, the threshold was changed from 0.05 to 0.046. After this adjustment, the bias was essentially zero (Figure 2-3).

Daily differences in extent are within +/-200,000 km^2 and the overall bias is -700 km^2 for the Arctic and 4700 km^2, both of which are well within the errors of the algorithm and input TB data. The concentrations were found to be within a few percent or less over most of the sea ice covered regions, with larger differences found only near the ice edge. Thus, the AMSR2 algorithm is well calibrated with AMSR-E and the validation studies done on AMSR-E products are valid for AMSR2 as well.

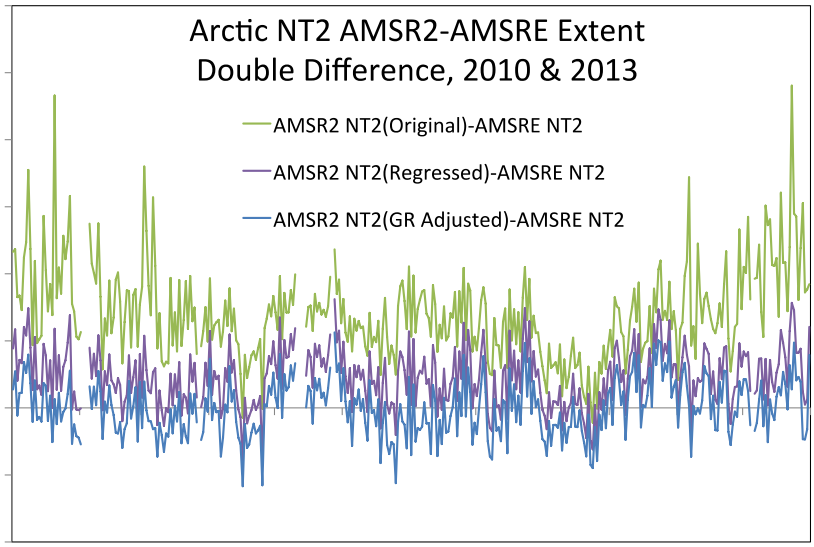

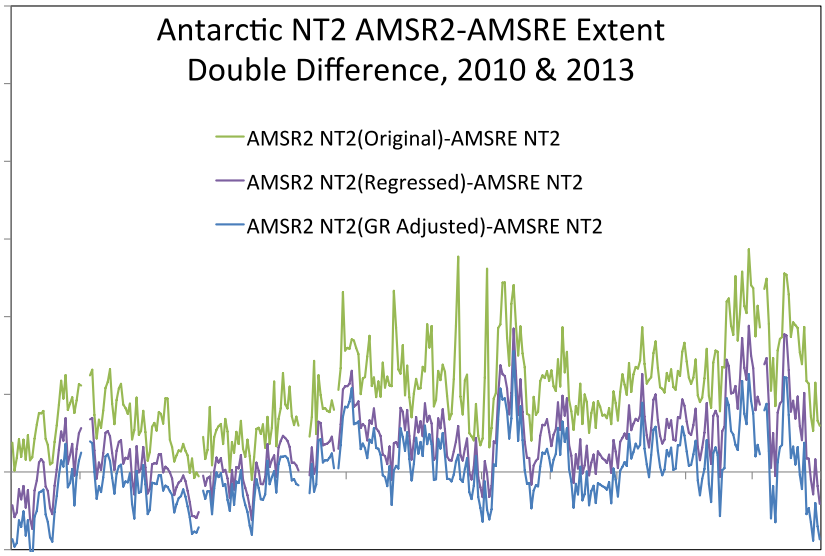

Figure 2-3. Daily extent difference between AMSR2-AMSR-E, using a double-difference approach with SSMIS, to demonstrate consistency between the NT2 algorithm output for both sensors.

2.5.2. Sea Ice Concentration Retrieval Errors

There are several sources of error for the SIC retrievals. First, there are uncertainties in the TB input data. However, these are calibrated to +/-1 K and the algorithms are not particularly sensitive to this small error. There is also error due to limitations in the sensor footprint resolution, which cannot directly resolve smaller-scale features; this is primarily an issue where there are large gradients in surface type: namely at the ocean-ice intersection and along the coast (primarily affecting open water coastal areas). As discussed above, a land-spillover correction is used to remove spurious ice along the coast. However, high uncertainties right at the ice edge are inevitable.

The more significant sources of error are ambiguities in surface properties and atmospheric emission. Atmospheric emission is corrected in NT2 using the radiative transfer model, though such corrections are clearly not perfect. Nonetheless, the TB frequencies used in the sea ice algorithm are relatively insensitive to atmospheric emission over the ice and most errors occur over open water, which are removed by the automated weather filter GR thresholds and the ocean SST mask.

Surface ambiguities are significant source of error, particular when melt occurs and the algorithms will have a tendency to interpret the surface water (and melt ponds) as reduced concentration ice. The NT2 algorithm is less sensitive to this effect than the original NT, but still can have some bias.

Thin ice is another regime with higher errors. Ice up to ~30 cm thick will be significantly underestimated or missed altogether. This primarily affects regions of new ice growth at the ice edge. Fortunately, ice growth is fairly rapid, so the bias disappears over a few days as the ice thickens. However, retrievals within a couple grid cells of the ice edge should be treated as suspect. Changes in snow depth, density, and grain size may also affect concentration are another source of uncertainty.

Overall, assessments have found that in cold, mid-winter conditions within the ice pack, concentrations are accurate to within 5% in comparison with high-resolution satellite data. For example, AMSR-E validation of NT2 concentration (Cavalieri et al., 2006) found differences of 1-5% in comparison with Landsat for thick, first-year ice during March in the Arctic. For thin ice near the ice edge, differences of ~15% (NT2 concentrations biased low) were found.

Bootstrap concentrations were found to have similar difference (Comiso and Nishio, 2008). However, because the two algorithms differ in their approach and use different TB channels, there is some independence between the two retrievals. When both algorithms yield very similar concentrations – generally in cold, mid-winter conditions within the pack – there is higher confidence in the NT2 estimates. When the algorithms yield differing estimates, it may be an indication of higher errors. Thus, the NT2-BT concentration

difference field provides and indication of uncertainty, albeit not a quantitative error estimate. Since the BT algorithm does not remove weather effects, such corrections to the data will also affect the difference field.

The multi-year ice concentration is currently a provisional product and has not been thoroughly validated. Comparison with independent sea ice age sources, such as Lagrangian tracked ice age, indicates overall good agreement in the spatial patterns of multi-year ice. However, users should consider the current MYIC product to be experimental.

2.6. Practical Considerations

2.6.1. Numerical Computation Considerations

It takes less than 360 seconds to process a full day of AMSR2 swaths (~28 half-orbits) for the sea ice product. This is based on the following CPU type “Intel(R) Core(TM) i7-2760QM CPU @ 2.40GHz”. This is more than sufficient to provide reasonable latency of the data products for users.

2.6.2. Programming and Procedural Considerations

The original code of AMSR2 sea ice retrieval algorithm is based on the NASA AMSR-E sea ice standard product code, written in a combination of Fortran 77 and C. The code has been updated to use non-proprietary compilers and software libraries (GNU gcc, gfortran, and NSIDC's Mapx grid transformation library). Fortran routines were updated to Fortran 90. Common blocks were removed, all compiler warnings were eliminated, and compiler optimization flags were turned on to improve runtime speed. Other significant changes to the code include using only the most recent observation at each grid cell. The output grid has been changed from the NSIDC 12.5 km polar stereographic to 10 km EASE2. NSIDC Mapx libraries are used for grid transformations. Ancillary data including the land mask, coast mask, and ocean SST masks have been prepared as static fields to save computational burden. All ancillary data are read at the beginning of the sea ice product retrieval procedure. AMSR2 brightness temperature swath data are read and processed individually to reduce memory overhead.

2.6.3. Quality Assessment and Diagnostics

The efforts will be continued to assess the AMSR2 sea ice products, using available comparison imagery such as LandSat-8, MODIS, and operational analyses such as IMS/MASIE (http://nsidc.org/data/masie). The MYIC will be validated via comparisons with Lagrangian sea ice age data and ASCAT scatterometry imagery.

2.6.4. Exception Handling

The exceptional cases--if they exist--will occur while reading the inputs of AMSR2 brightness temperature and other ancillary data. Fatal errors within AMSR2 Brightness Temperatures may cause weird sea ice property retrieval but these errors are very unlikely. The ancillary files are static so read errors with the ancillary data are very unlikely. Once the quality of AMSR2 Brightness Temperature data is confirmed and the computing facility is stable, the frequency of exceptional cases will be rare.

2.7. Concentration Product Validation

As mentioned above, the NT2 algorithm has been well validated through its development as the NASA AMSR-E standard sea ice concentration product. Overall, assessments have found that in cold, mid-winter conditions within the ice pack, concentrations are accurate to within 5% in comparison with high-resolution satellite data. For example, Andersen et al. (2007) compared several algorithms, including NT2 with high-resolution SAR data in the central Arctic during winter (31 October to 31 March). For high concentration (>90%) ice typical in the high Arctic, they found error standard deviations of only 1.7-1.8%. To some degree this is because when the concentrations are very high (generally 95-100%) and since the algorithm cuts off concentrations at 100%, the error profile is not symmetric. When concentrations greater than 100% are allowed, error standard deviation rises to 5.0-5.5%. However, for practical considerations, since concentrations cannot exceed 100%, the lower error value is reasonable. In all concentration regimes (including <90%), the NT2 error standard deviation was 4.9%. Andersen et al. (2007) evaluated NT2 for SSMI data. With higher spatial resolution, AMSR2 errors would be expected to be lower, especially in lower concentrations, where sensor resolution is more critical.

The NT2 concentration retrievals for AMSR-E were specifically validated by Cavalieri et al. (2006) via comparison with Landsat-7 ETM+ imagery. They found differences of 1-5% in comparison with Landsat for thick, first-year ice during March in the Arctic. For new/thin ice near the ice edge or in polynyas (open water regions within the ice cover), differences of up to ~15% (NT2 concentrations biased low) were found. Performance varied considerably depending on the specific conditions, but the high errors were nearly all found in new ice regimes. This is not surprising given the high variability of new ice, both spatial and temporally. For example, the AMSR-E concentrations were daily averages, while the Landsat-7 imagery were specific swaths. Thus, an AMSR-E observation could potentially be separated from the Landsat image by nearly 24 hours. Significant ice growth can occur in that time. The use of “latest” observation in this product will eliminate this “time-smearing” error. New ice also tends to be highly spatially variable and in a narrow (a few grid cells at most) region near the ice edge (or in polynyas). Thus significant differences between AMSR-E and Landsat spatial resolution affect the error estimates (Figure 2-4).

The multi-year ice concentration is currently a provisional product and has not been thoroughly validated. Comparison with independent sea ice age sources, such as Lagrangian-tracked ice age (Tschudi et al., 2015; Maslanik et al., 2011), indicates overall good agreement in the spatial patterns of multi-year ice. For example, the spatial pattern of MYI in AMSR2 generally corresponds well with the location of ice with age >1 year old. The AMSR2 MYIC algorithm does sometimes detect thin ice (e.g. Bering Sea) as MYI because their microwave signatures are similar at the algorithm frequencies. However, these false retrievals can be filtered by applying a regional mask. Further validation is planned with the Lagrangian fields and with ASCAT scatterometer fields. Thus, for the initial version of the product, the MYIC fields are provisional.

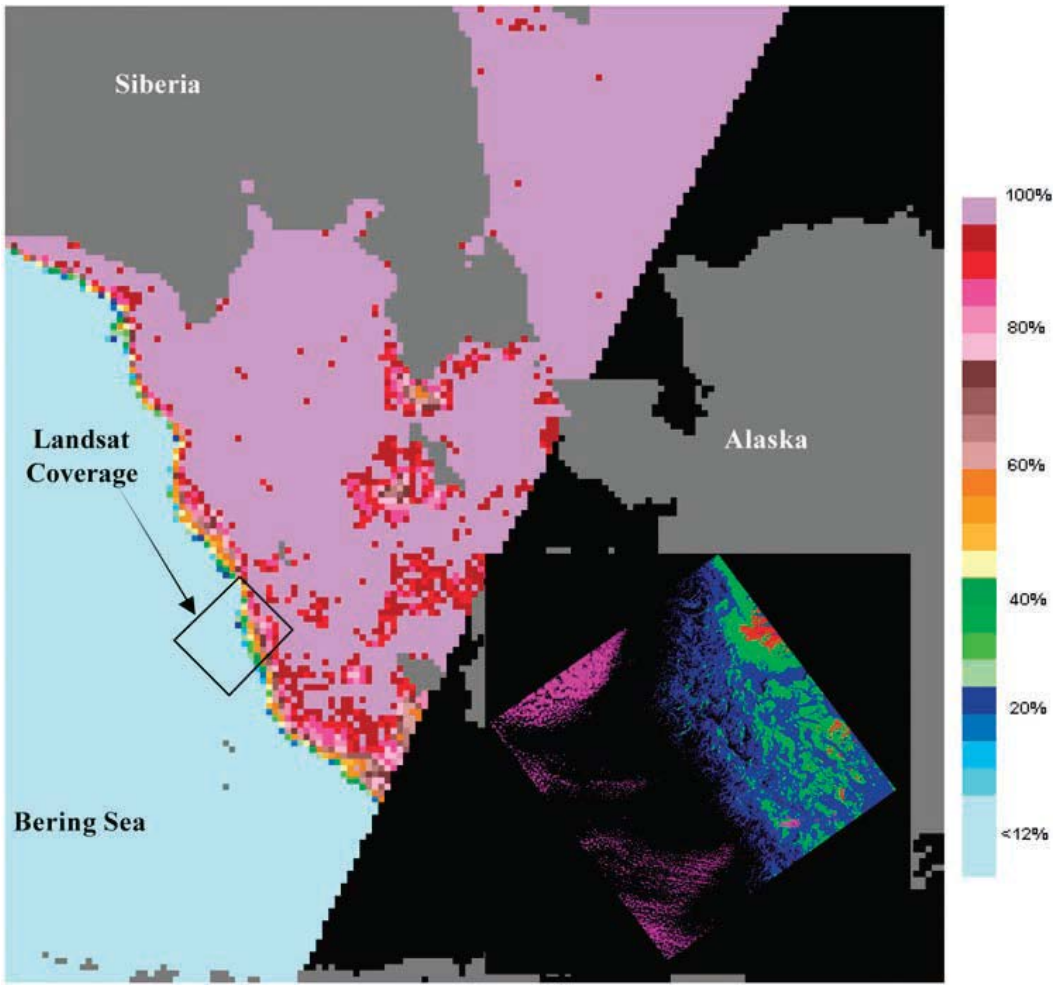

Figure 2-4: AMSR-E sea ice concentration in the Bering Sea on March 22, 2003, with Landsat-7 ETM+ region boxed. Inset: Landsat-7 classified image. Red corresponds to FYI, green to young ice, and blue to new ice; black is open water and pink corresponds to clouds. From Cavalieri et al. (2006) (Figure 6).

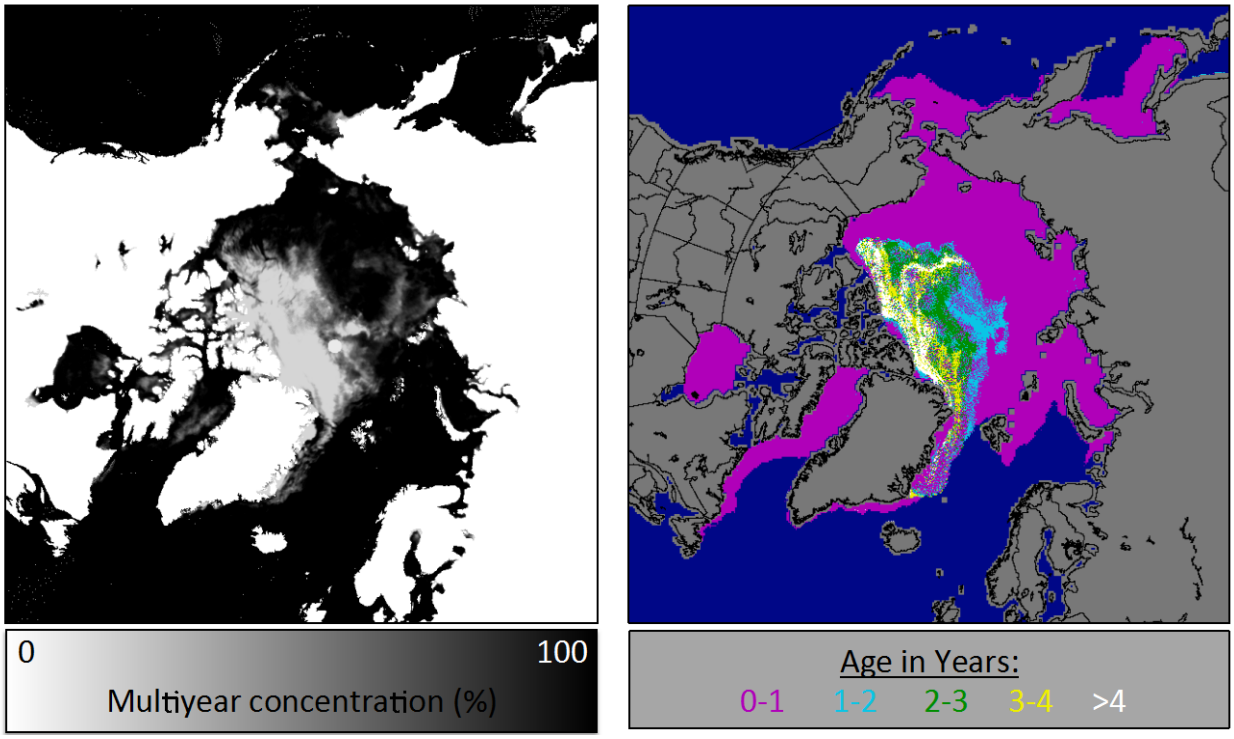

Figure 2-5: AMSR2 MYIC (right) for 15 March 2015 in the Arctic with synchronous Lagrangian ice age product (left).

3. ASSUMPTIONS AND LIMITATIONS

3.1. Performance Assumptions

Based on the numerous assessments of the AMSR-E and AMSR2 sea ice products generated by the AMSR2 sea ice retrieval algorithm, the AMSR2 sea ice retrieval algorithm should work within the accuracy range shown in the Algorithm Readiness Review (ARR) for most cases. Regions where errors may exceed the ARR accuracy are: thin ice (< 30 cm) within a few days of formation, near the ice edge (within ~50 km), under heavy melt conditions. Higher errors may rarely occur in other situation due to anomalous conditions (e.g., snow transformation melt/refreeze). Also, the weather filters, ocean SST mask, and land-spillover correction may not remove all spurious ice, so spurious ice may be found in clearly ice-free regions along the coast and in the open ocean far from the ice edge.

3.2. Potential Improvements

There are several potential improvements to the product, but most of these are longer-term research level endeavors beyond the scope of this project. These include: improved

atmospheric correction using atmospheric reanalyses, development of quantitative uncertainty estimates. More basic improvements could include: use of daily SST maps instead climatology for the SST mask, use of the higher resolution 89 GHz to produce 5 km resolution gridded fields. Refinements to the MYIC parameterization are also feasible.

4. REFERENCES

Andersen, S., R. Tonboe, S. Kern, and H. Schyberg, 2006: Improved retrieval of sea ice total concentration from spaceborne passive microwave observations using numerical weather prediction model fields: An intercomparison of nine algorithms, *Rem. Sens. Env.*, 104: 374-392.

Andersen, S., R. Tonboe, L. Kaleschke, G. Heygster, and L.T. Pedersen, 2007: Intercomparison of passive microwave sea ice concentration retrievals over the high-concentration Arctic sea ice, *J. Geophys. Res.*, 112, C08004, doi:10.1029/2006JC003543.

Brodzik, M. J., and K. Knowles. 2011. *EASE-Grid 2.0 Land-Ocean-Coastline-Ice Masks Derived from Boston University MODIS/Terra Land Cover Data*. Boulder, Colorado USA: NASA National Snow and Ice Data Center Distributed Active Archive Center. http://dx.doi:10.5067/VY2JQZL9J8AQ.

Brodzik, M. J., B. Billingsley, T. Haran, B. Raup, M. H. Savoie, 2012: EASE-Grid 2.0: Incremental but significant improvements for earth-gridded data sets. *ISPRS International Journal of Geo-Information*, 1(1):32-45, doi:10.3390/ijgi1010032. http://www.mdpi.com/2220-9964/1/1/32/.

Brodzik, M. J., B. Billingsley, T. Haran, B. Raup, M. H. Savoie, 2014: Correction: Brodzik, M. J. et al. EASE-Grid 2.0: Incremental but significant improvements for earth-gridded data sets. *ISPRS International Journal of Geo-Information* 2012, 1, 32-45. ISPRS International Journal of Geo-Information, 3(3):1154-1156, doi:10.3390/ijgi3031154. http://www.mdpi.com/2220-9964/3/3/1154/.

Cavalieri, D.J., P. Gloersen, and W.J. Campbell, 1984: Determination of sea ice parameters with the Nimbus-7 Scanning Multichannel Microwave Radiometer. *J. Geophys. Res.*, **89**, 5355-5369.

Cavalieri, D.J., T. Markus, D.K. Hall, A.J. Gasiewski, M. Klein, and A. Ivanoff, 2006: Assessment of EOS Aqua AMSR-E Arctic sea ice concentrations using Landsat-7 and airborne microwave imagery. *Trans. Geosci. Rem. Sens.*, **44(11)**, 3057-3069, doi:10.1109/TGRS.2006.878445.

Comiso, J.C., D.J. Cavalieri, and T. Markus, 2003: Sea ice concentration, ice temperature, and snow depth using AMSR-E data. *IEEE Trans. Geosci. Rem. Sensing*, **41(2)**, 243-252: doi:10.1109/TGRS.2002.808317.

Comiso, J.C., and F. Nishio, 2008: Trends in the Sea Ice Cover Using Enhanced and Compatible AMSR-E, SSM/I, and SMMR Data. *J. of Geophys. Res.,* 113, C02S07, doi:10.1029/2007JC0043257.

Comiso, J.C., 2009: Enhanced sea ice concentrations and ice extents from AMSR-E Data. *J. Rem. Sens. of Japan,* 29(1), 199-215.

Chang, P., T. King, L. Soulliard, and Z. Jelenak, 2012: GCOM-W1, AMSR2 Algorithm Software Processor (GAASP) Package: Preliminary Design Review, Nov. 8, 2012, GAASP Preliminary Design Review.

Eppler, D.T., and 14 others, 1992: Passive microwave signatures of sea ice, in "Microwave Remote Sensing of Sea Ice." F.D. Carsey, ed., *American Geophysical Union Monograph* 68, Washington, DC, 47-71.

Fraser R. S., N. E. Gaut, E. C. Reifenstein, and H. Sievering, 1975: Interaction mechanisms within the atmosphere including the manual of remote sensing, *American Society of Photogrammetry,* 181-233, Falls Church, VA.

Friedl, M. A., et al. 2002. Global Land Cover Mapping from MODIS: Algorithms and Early Results. Remote Sensing of the Environment 83: 287-302.

Imaoka, K., M. Kachi, M. Kasahara, N. Ito, K. Nakagawa, and T. Oki, 2010: Instrument performance and calibration of AMSR-E and AMSR2, *Proc. Int. Archives of the Photogrammetry, Rem. Sens. and Spatial Information Science*, vol. XXXVIII, Part 8.

Ivanova, N., O.M. Johannessen, L.T. Pedersen, and R.T. Tonboe, 2014: Retrieval of Arctic sea ice parameters by satellite passive microwave sensors: A comparison of eleven sea ice concentration algorithms, *IEEE Trans. Geosci. Rem. Sens.*, 52(11), 7233-7246, doi:10.1109/TGRS.2014.2310136.

Ivanova, N., L.T. Pedersen, R.T. Tonboe, S. Kern, G. Heygster, T. Lavergne, A. Sorensen, R. Saldo, G. Dybkjaer, L. Brucker, and M. Shokr, 2015. Inter-comparison and evaluation of sea ice algorithms: towards further identification of challenges and optimal approach using passive microwave observations, *The Cryosphere*, 9, 1797-1817, doi:10.5194/tc-9-1797-2015.

Kummerow, C., 1993: On the Accuracy of the Eddington Approximation for Radiative Transfer in the Microwave Frequencies. *J. Geophys. Res.,* 98, 2757-2765.

Levitus, S. and Boyer, T.P., 1994: World Ocean Atlas 1994, Volume 4: Temperature, NOAA National Oceanographic Data Center, Ocean Climate Laboratory, U.S. Department of Commerce, Washington D.C.

Markus, T., and D.J. Cavalieri, 2000: An enhancement of the NASA Team sea ice algorithm. *IEEE Trans. Geosci. Rem. Sens.*, **38(3)**, 1387-1398.

Markus, T., and D.J. Cavalieri, 2009: The AMSR-E NT2 sea ice concentration algorithm: it's basis and implementation. *J. Rem. Sens. Japan*, **29(1)**, 216-225.

Maslanik, J., J. Stroeve, C. Fowler, and W. Emery, 2011. Distribution and trends in Arctic sea ice age through spring 2011. *Geophys. Res. Lett.*, 38(L13502). doi: 10.1029/2011GL047735.

Meier, W.N., 2005: Comparison of passive microwave ice concentration algorithm retrievals with AVHRR imagery in Arctic peripheral seas, *IEEE Trans. Geosci. Remote Sens.*, 43(6), 1324-1337.

Tschudi, M., C. Fowler, and J. Maslanik, 2015. *EASE-Grid Sea Ice Age, Version 2*. Boulder, Colorado USA. NASA National Snow and Ice Data Center Distributed Active Archive Center. http://dx.doi.org/10.5067/1UQJWCYPVX61.

END OF DOCUMENT